RESEARCH ARTICLE

WILEY

Ecohydrological implications of aeolian sediment trapping by sparse vegetation in drylands

Howell B. Gonzales¹ | Sujith Ravi¹ | Junran Li² | Joel B. Sankey³ |

Correspondence

Sujith Ravi, Department of Earth and Environmental Science, Temple University, Philadelphia, PA 19122, USA. Email: sravi@temple.edu

Funding information

U.S. National Science Foundation (NSF), Grant/Award Numbers: EAR-1451489 and EAR-1451518

Abstract

Aeolian processes are important drivers of ecosystem dynamics in drylands, and important feedbacks exist among aeolian-hydrological processes and vegetation. The trapping of wind-borne sediments by vegetation canopies may result in changes in soil properties beneath the vegetation, which, in turn, can alter hydrological and biogeochemical processes. Despite the relevance of aeolian transport to ecosystem dynamics, the interactions between aeolian transport and vegetation in shaping dryland landscapes where sediment distribution is altered by relatively rapid changes in vegetation composition such as shrub encroachment, are not well understood. Here, we used a computational fluid dynamics modelling framework to investigate the sediment trapping efficiencies of vegetation canopies commonly found in a shrub-grass ecotone in the Chihuahuan Desert (New Mexico, USA) and related the results to spatial heterogeneity in soil texture and infiltration measured in the field. The vegetation structures were created using a computer-aided design software, with inherent canopy porosities, which were derived using Light Detection and Ranging (LiDAR) measurements of plant canopies. Results show that considerable heterogeneity in infiltration and soil grain size distribution exist between the microsites, with higher infiltration and coarser soil texture under shrubs. Numerical simulations further indicate that the differential trapping of canopies might contribute to the observed heterogeneity in soil texture. In the early stages of encroachment, the shrub canopies, by trapping coarser particles more efficiently, might maintain higher infiltration rates leading to faster development of the microsites with enhanced ecological productivity, which might provide positive feedbacks to shrub encroachment.

KEYWORDS

CFD, grain size distribution, infiltration, sediment transport, trapping efficiency, wind erosion

1 | INTRODUCTION

Aeolian processes, the erosion, transport, and deposition of sediment by wind, are recognized as important abiotic drivers in the Earth's system, with implications on landscape evolution, biogeochemical cycles, climate, air quality, and desertification (Field et al., 2010; Ravi et al., 2011). Aeolian processes are dominant in many arid and semi-arid regions of the world which are characterized by low annual precipitation and exhibit soils with sparse patchy vegetation cover (Breshears, Whicker, Johansen,

& Pinder, 2003). In these landscapes, aeolian processes are especially responsible for the erosion of fine sediments from unvegetated soil surfaces and the downwind deposition beneath vegetation canopies (Li, Okin, Alvarez, & Epstein, 2009; Okin & Gillette, 2001; Ravi, Breshears, Huxman, & D'Odorico, 2010). On the other hand, the structure and distribution of vegetation and other non-erodible roughness elements is a dominant control over the rate and patterns of erosion and redistribution by wind (Wolfe & Nickling, 1993; Okin & Gillette, 2001; Raupach, Woods, Dorr, Leys, & Cleugh, 2001; Li, Okin, Alvarez, & Epstein, 2007).

¹ Department of Earth and Environmental Science, Temple University, Philadelphia, PA 19122, USA

² Department of Geosciences, The University of Tulsa, Tulsa, OK 74104, USA

³ Southwest Biological Science Center, Grand Canyon Monitoring and Research Center, U.S. Geological Survey, Flagstaff, AZ 86001, USA

Dryland vegetation patches can trap wind- and water-borne sediments, resulting in sediment deposition under vegetated patches and the subsequent development of areas of enhanced hydrological and biogeochemical productivity, which are distributed between areas of nutrient depleted bare interspaces (Charley & West, 1977; Puigdefabregas, 2005; Schlesinger et al., 1990). In some dryland ecosystems, aeolian processes are dominant and their role in the formation and maintenance of these "islands of fertility" is well documented (Okin & Gillette, 2001; Ravi, D'Odorico, & Okin, 2007; Li, Okin, Alvarez, & Epstein, 2008). However, the sediment trapping efficiencies of vegetation canopies—herein defined as the proportion of the total aeolian sediment removed from transport due to canopy effect on windflow and sediment—vary by the particle size distribution (PSD) of the entrained sediment and the aerodynamic properties of the vegetation species including canopy porosity and geometry (Raupach et al., 2001). Thus, the differential trapping of wind-borne sediment by dryland vegetation may in turn lead to heterogeneity in the spatial patterning of soil, nutrient, and hydrologic properties at the scale of vegetated microsites and bare interspaces. In many dryland systems, the coppice and interspace variation in soil properties is a key aspect in understanding ecosystem processes including plant community changes (e.g., invasion or encroachment) and the response to management and restoration practices (Bhark & Small, 2003; Hoover & Germino, 2012; Li & Ravi, 2018; Puigdefabregas, 2005; Sankey, Germino, Sankey, & Hoover, 2012; Sankey, Ravi, Wallace, Webb, & Huxman, 2012; Schlesinger et al., 1990; Wang et al., 2018).

Despite the relevance of aeolian-vegetation interactions to ecosystem dynamics, the interactions between these two processes in landscapes undergoing rapid land-use changes or recurrent disturbances, or even longer-term succession, is not well understood. In particular, aeolian-vegetation interactions are important in shaping dryland landscapes where sediment distribution is altered by relatively rapid changes in vegetation composition (Okin & Gillette, 2001; Li et al., 2008). A case in point is the encroachment of shrubs into areas historically dominated by grasses, which is documented worldwide and is often considered a manifestation of land degradation (Archer, Schimel, & Holland, 1995; Schlesinger et al., 1990; Van Auken, 2000). The grass-shrub vegetation shifts are attributed to a variety of factors including natural and anthropogenic disturbances, overgrazing, less frequent fires, and microclimatic modification by shrubs (Coetzee, Tincani, Wodu, & Mwasi, 2008; He, D'Odorico, De Wekker, Fuentes, & Litvak, 2010; Scholes & Archer, 1997; Van Auken, 2000). Overall, shrub encroachment results in the development of a heterogeneous patchy landscape with nutrient-enriched shrub microsites interspaced between nutrient-depleted bare interspaces, with implications for ecohydrological, geomorphological, and biogeochemical processes (Huxman et al., 2005; Okin & Gillette, 2001; Sankey, Germino, et al., 2012; Sankey, Ravi, et al., 2012; Schlesinger et al., 1990; Wilcox & Thurow, 2006). The landscapes undergoing vegetation shifts from grass to shrub may experience accelerated soil erosion, due to increased bare patches between the vegetation (Okin et al., 2009). Aeolian processes, in particular, are thought to play a major role in the formation and development of the islands of fertility by the removal of sediments from interspaces and the subsequent redistribution onto the shrub-vegetated microsites.

Traditional field methods to quantify the parameters related to the sediment trapping efficiencies of vegetation canopies can be challenging, as both the characteristics of the canopy (i.e., geometry, porosity), and the sediment deposition is difficult to quantify. Fortunately, there is an alternative way to predict windflow and sediment trapping associated with the growth forms of different plant species by implementing numerical modelling through computational fluid dynamics (CFD) simulation. A number of studies using various types of vegetation models (natural or artificial) were conducted in the past as a validation for numerical modelling using commercially available software (e.g., Bitog et al., 2012; Endalew et al., 2009; Gromke, Buccolieri, Di Sabatino, & Ruck, 2008; Guo & Maghirang, 2012; Lin, Barrington, Choinière, & Prasher, 2007; Rosenfeld, Marom, & Bitan, 2010; Tiwary, Morvan, & Colls, 2006). The GNU Public License provides alternative CFD open-source software packages that can be freely downloaded and shared through the internet (e.g., OpenFOAM, 2015).

Here, we assessed the trapping efficiencies of shrub and grass species commonly associated with shrub encroachment into grasslands in the northern Chihuahuan Desert using a novel CFD approach. We conducted infiltration experiments and analysed PSD of soils at microsites beneath several individuals of both species and used ground-based Light Detection and Ranging (LiDAR; Sankey, Law, Breshears, Munson, & Webb, 2013) to quantify their typical canopy porosities. We created three-dimensional (3D) architectural depictions of each species using an open-source computer-aided design software (Blender®). We, then, used these data in an open-source CFD software (OpenFOAM®) program to assess trapping efficiencies of the two species of vegetation against aeolian sediment flux. The potential ecohydrological implications of the differential aeolian sediment trapping of shrub and grass canopies are discussed.

2 | METHODS

2.1 | Field and laboratory soil analysis

Field experiments were conducted at the Sevilleta National Wildlife Refuge (New Mexico, USA) in the northern Chihuahuan Desert. The study site is located in a shrub-grass ecotone (lat/long: 34.33°N, 106.72°W) composed of Black Grama (Bouteloua eriopoda) dominated grassland with Creosote (Larrea tridentata) shrubs (Figure 1). The study area is characterized by flat topography, and the shrub microsites are in the early stage of development with less microtopographic relief compared to areas with well-developed shrub islands (Dukes et al., 2018). The predominant wind in this location during the windy season (February to May) is from the southwest (Dukes et al., 2018). The annual long-term average precipitation at the site is 250 mm, and up to 80% of the precipitation occurs during the summer months (Muldavin, 2002).

Infiltration experiments were conducted in three distinct microsites—shrub, grass, and bare soil interspace. For the grass microsites, the infiltration measurements were taken inside the grass patch, depending on the ease of installing the infiltrometer. For the shrub microsites, to maintain consistency, the measurements were taken on the southwest side under the shrub canopy within



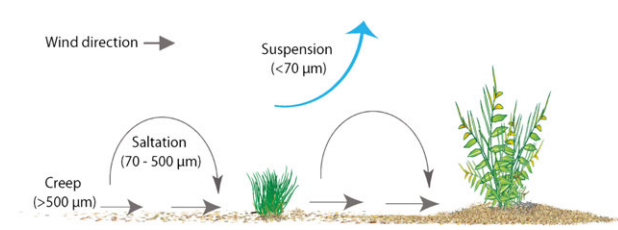


FIGURE 1 (a) The shrub-grass ecotone at the Sevilleta National Wildlife Refuge, New Mexico. (b) A conceptual depiction of aeolian sediment trapping by vegetation

25 cm from the base of the shrub. Field saturated hydraulic conductivity (K_{sat}) was estimated using a portable dualhead infiltrometer (Decagon Services, Pullman, WA), which measures K_{sat} using a modified two-ponding head approach (Nimmo, Schmidt, Perkins, & Stock, 2009; Reynolds & Elrick, 1990). The infiltrometer has an inner diameter of 14.4 cm and insertion depth of 5 cm. This device has an infiltration rate range of 0.0038-115 cm hr⁻¹, with a resolution of 0.0038 cm hr⁻¹ and an accuracy of ±5%. The fully automated infiltrometer can produce variable hydraulic conductivity conditions without varying the water depth by using air pressure to create different pressure heads. It maintains the steady water levels and measures infiltration rates through two complete pressure cycles. The data are collected by a control unit that performs the calculations to determine field saturated hydraulic conductivity. The K_{sat} was measured on five randomly selected shrub, grass, and bare microsites each (5 × 3 replicates). Unsaturated hydraulic conductivity (K at 2 cm suction) was measured using the mini disk infiltrometer (Decagon Devices, WA, USA) following the method of Zhang (1997). The infiltrometer has an adjustable suction and a small footprint (measuring area of 5 cm diameter porous stainless-steel disc) and is ideal for measuring the variability of unsaturated hydraulic conductivity of each microsite. The unsaturated hydraulic conductivity was measured on 10 randomly selected shrub, grass, and bare microsites each (10 × 3 replicates).

Soil samples were collected from the top 2 cm of the soil profile for six shrub, grass, and bare interspaces (6×3 replicates). In the laboratory, soil samples were air-dried and sieved using a 2-mm sieve and split into 2-g subsamples using a riffle sampler (Humboldt Mfg. Co. IL, USA). The samples were treated with sodium hypochlorite (24 hr) to digest the organic matter. The PSD of soils was determined using a laser-diffraction grain size analyzer (LS 13 320 Particle Size Analyzer, Beckman Coulter, Inc, CA, USA) with a dynamic measurement range

of 0.017–2,000 μ m. Grain-size statistics and parameters (median [ϕ], mean [ϕ], and sorting) were obtained by using the results of the laser diffraction analysis and equations presented by Folk (1980). The phi unit (ϕ) is a logarithmic transformation of millimetres into whole integers (ϕ = $-\text{Log}_2$ d, where d is the grain diameter in mm). The median grain size (ϕ ₅₀) corresponds to the 50th percentile of a grain sample by weight in phi units. The average grain-size or mean was derived using the graphical mean (M_z) equation as follows:

$$M_z = \frac{\Phi_{16} + \Phi_{50} + \Phi_{84}}{3},\tag{1}$$

where ϕ_{16} , ϕ_{50} , and ϕ_{84} represent sizes at 16th, 50th, and 84th percentiles of the grain sample by weight. Sorting (σ_1) is a measure of variation in grain sizes and is based on the inclusive standard deviation introduced by Folk (1980) and is computed as follows:

$$\sigma_1 = \frac{\Phi_{84} - \Phi_{16}}{4} - \frac{\Phi_{95} - \Phi_5}{6.6},\tag{2}$$

where ϕ_{84} , ϕ_{16} , ϕ_{95} , and ϕ_{5} represent sizes at 84th, 16th, 95th, and 5th percentiles of the grain sample by weight.

The threshold shear velocity (TSV) of soil particles from the bare microsites (the dominant source of aeolian sediments) was estimated using an empirical method developed by Li et al. (2010). In this method, TSV was estimated with the resistance of the soil surface to disturbances created by a penetrometer and projectile shot (at 45° to the soil surface) by air gun at the soil. The TSV measurements (n = 5) were conducted prior to the infiltration measurements and soil sampling when the soil surface was not disturbed. More details about this method, including the accuracy of TSV estimates from the same sites, may be found in Dukes et al. (2018).

Statistical tests (One-way ANOVA and TUKEY HSD, *R* version 3.2.4, 2016) were conducted to test the significance of differences in hydraulic conductivity and PSD among different microsites.

2.2 | Wind profiles

Wind profiles were obtained at the site using the wind speeds measured by four anemometers (Model 03101 RM Young, MI, USA) mounted at incremental heights above ground (0.5, 1, 2, and 4 m) on a stationary tower. Wind speeds were recorded continuously using a datalogger (Model CR1000, Campbell Scientific, UT, USA).

2.3 | Vegetation porosity determination

Typical porosities of shrub and grass were estimated using LiDAR data acquired with a Riegl VZ1000 laser scanner mounted on a tripod. Nine individual creosote shrubs and nine individual black grama grass bunches were scanned from two opposing scan locations or sides of each plant during March 2016. The individual plants of each species were selected with equal representation from three undisturbed (control) study plots described in detail in Dukes et al. (2018). For each individual plant, the two scan datasets were coregistered to produce a single point cloud dataset of LiDAR returns. Each point cloud dataset was edited to remove LiDAR returns from the ground surface and then octree-filtered to decimate the data such that there was no

more than one point (LiDAR return from vegetation) per 1 cm³. Then, porosities of the individual plant canopies were estimated by first estimating the volume of a cylinder that would contain the plant as:

Volume
$$(cm^3) = \pi^* Canopy \ radius^{2*} Plant \ height$$
 (3)

and then

Porosity (%) =
$$\left[1-\left[\text{Lidar point count/Volume}\right]\right]*100$$
, (4)

where LiDAR point count is the number of LiDAR returns from vegetation in the filtered point cloud dataset. All processing and analysis of the LiDAR data was completed in RiscanPro software. The ranges of canopy porosity estimates were 80–90% for the Creosote shrubs and 65–75% for the Black Grama grasses.

2.4 | Numerical simulation

Numerical simulation through CFD modelling involved three stages of operations: preprocessing, processing, and post-processing. The preprocessing stage created the geometry and computational domain combined with the generation of the computational mesh. The mesh created for this study was for an external flow (outside the 3D computer-aided design model). The processing stage involves the selection of a specific solver based on the discretization schemes considered for the governing equations of the problem to be solved. In the post-processing stage, the data were visualized using charts, graphs, and contour plots. We used an open-source software, OpenFOAM® (ver. 4.0, ESI-OpenCFD, openfoam.org).

The porosity data obtained using the LiDAR were used to construct the 3D geometries of shrub and grass. The computational domain for the external flow simulation generated from the blockMesh and snappyHexMesh tools of the OpenFOAM is given in Figure 2 with the direction of airflow as indicated. The face boundaries of the computational domain were named as inlet (-x axis), outlet (+x axis), frontAndback (-y and +y axes), upperWall (z = H), and lowerWall (z = 0), which were in accordance to the direction of air flow (-x axis to +x axis) for simulation purposes. Due to the intensive computational power required for complex structures of shrub and grass canopy, only a single vegetation element was considered for the domain. The length and height of the elements were dictated by the computational time required for computing wind speeds across the vegetation.

A simplified numerical simulation approach was investigated to identify the efficiency of two representative plants, that is, creosote shrub and black grama grass in trapping soil particles during the process of aeolian sediment transport. The air flow through the shrub and the grass adapts the Reynolds-averaged Navier–Stokes (RANS) instantaneous multiple component velocities approach. The 3D geometries of the shrub and grass also requires the use of the 3D RANS steady-state, incompressible, isothermal, and neutrally stratified turbulent atmospheric layers as assumptions for the airflow (Guo & Maghirang, 2012) while ignoring mass transfer. During the process of a wind event, the continuity and conservation of momentum may be described as (Cheng, Lien, Yee, & Sinclair, 2003; Endalew et al., 2009; Yeh, Tsai, & Yang, 2010):

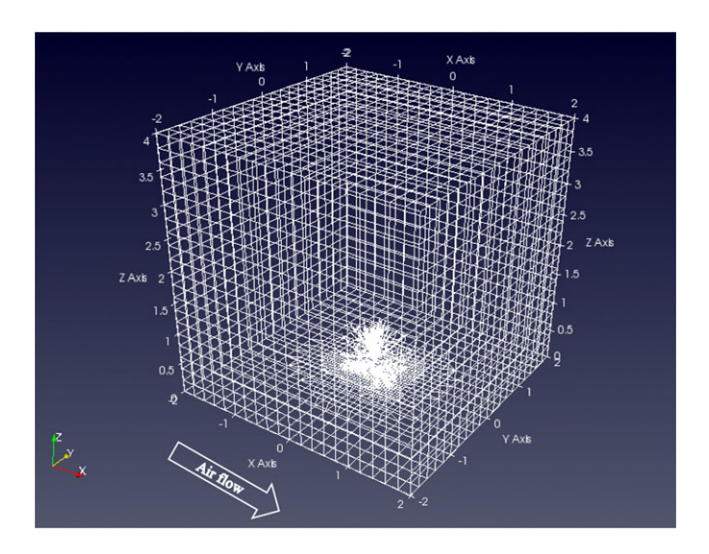


FIGURE 2 Computational domain for airflow and dust flow through shrub using ParaView (Ver. 5.3, paraview.org)

$$\partial \frac{\overline{u_i}}{\partial x_i} = 0 (5)$$

$$\frac{\partial u_{i}u_{j}}{\partial x_{j}} = -\frac{1}{\rho}\frac{\partial \rho}{\partial x_{i}} + \frac{1}{\rho}\frac{\partial}{\partial x_{j}}\mu\left(\frac{\partial u_{i}}{\partial x_{j}} + \frac{\partial u_{j}}{\partial x_{i}}\right) - \frac{\partial}{\partial x_{j}}\left(\overline{u_{i}^{'}u_{j}^{'}}\right),\tag{6}$$

where *i* is the subscript for all three directions (x, y, and z), j is the subscript for the direction evaluated (x, y, or z), u is the velocity (m s⁻¹), p is the pressure force (Pa) in *i*-direction evaluated, and μ is the fluid viscosity (N s m⁻²).

The two-equation RANS-based model, the RNG *k*-model, was used for the numerical simulations for this study and is given by the following equations (Bitog et al., 2012; Yeh et al., 2010):

$$\frac{\partial}{\partial x_{i}}(\rho k u_{i}) = \frac{\partial}{\partial x_{j}} \left[\alpha_{k} \mu_{eff} \frac{\partial k}{\partial x_{i}} \right] + G - \rho \epsilon \tag{7}$$

$$\frac{\partial}{\partial x_{i}}(\rho\epsilon u_{i}) = \frac{\partial}{\partial x_{j}}\left[\alpha_{\epsilon}\mu_{\text{eff}}\frac{\partial\epsilon}{\partial x_{i}}\right] + C_{1\epsilon}\frac{\epsilon}{k}\left(G\right) - C_{2\epsilon}^{*}\rho\frac{\epsilon^{2}}{k} \tag{8}$$

$$G = 2\mu_t S_{ij} S_{ij} \tag{9}$$

$$\mu_{t} = \rho C_{\mu} \frac{k^{2}}{\varepsilon}, \tag{10}$$

where μ_{eff} is the effective viscosity (N s m⁻²), k is the turbulence kinetic energy (m² s⁻²), ε is the turbulence dissipation rate (m² s⁻³), α_k is the Prantdl number of the turbulence kinetic energy, α_{ε} is the Prantdl number of the turbulence dissipation rate, $C_{1\varepsilon}$ is a turbulence model constant equal to 1.42, S_{ij} is the strain rate tensor, and μ_t is the turbulent viscosity (N s m⁻²). Meanwhile, $C_{2\varepsilon}^*$ is obtained as follows:

$$C_{2\varepsilon}^* = C_{2\varepsilon} + C_{2\varepsilon}' \tag{11}$$

with $C_{2\varepsilon}$ as the turbulence model constant equal to 1.68 whereas $C_{2\varepsilon}^{'}$ is determined using the equation:

$$C_{2\varepsilon}^{'} = \frac{C_{\mu}\rho\eta^{3}(1-\eta/\eta_{0})}{1+\beta\eta^{3}}$$
 (12)

with η_o as a constant equal to 4.38 whereas η is obtained by using the equation:

 $\eta = S \frac{k}{c} \tag{13}$

$$S = \sqrt{2S_{ij}S_{ij}} \tag{14}$$

The RNG $k-\varepsilon$ model was found to be the best turbulence model for investigation of complex wind flows around barriers in a number of studies (Bitog et al., 2012; Bourdin & Wilson, 2008; Lee & Lim, 2001; Packwood, 2000; Lee, Sase, & Sung, 2007; Li et al., 2007; Santiago, Martín, Cuerva, Bezdenejnykh, & Sanz-Andrés, 2007; Yeh et al., 2010). The transport of particles across the 3D vegetation was modelled using the Eulerian approach, which treats the passing stream of particles as one continuum. A convection-diffusion equation (a scalar transport equation) was used for soil particles flow through the shrub and grass (OpenFOAM, 2015):

$$\frac{\partial}{\partial x_{i}}(u_{i}C) - \frac{\partial^{2}}{\partial x_{i}^{2}}(\Gamma_{D}C) = 0, \tag{15} \label{eq:15}$$

where C is dust concentration and Γ_D is effective diffusion coefficient of dust particles. The wind speed values required for the particle transport calculation in Equation (5) is obtained from the results of the simpleFoam solver simulations, which essentially solves for the wind velocity fields. The assumption made here is that the amount of reduction of particles of specific sizes at the wake of the canopy is the reduction of particle concentration of that size. Furthermore, $\Gamma_D = \Gamma_L + \Gamma_T$ where Γ_L is the laminar component while Γ_T is the turbulent component. Γ_L is computed using the Stoke–Einstein equation (Guo & Maghirang, 2012):

$$\Gamma_L = \frac{\zeta T C_c}{3\pi \mu d_p},\tag{16}$$

where ζ is the Boltzmann constant, T is absolute temperature (K), C_c is the slip correction factor, d_p is particle diameter. The term C_c may be found using the following equation:

$$C_{C} = 1 + \frac{\lambda}{d_{p}} \left[2.34 + 1.05 \exp\left(-\frac{0.39d_{p}}{\lambda}\right) \right], \tag{17}$$

where λ is the mean free path (μ m). The parameter Γ_T is computed according to

$$\Gamma_{T} = \frac{\left(\frac{\rho C_{\mu} k}{\varepsilon}\right)}{S_{C_{t}}},\tag{18}$$

where Sc_t is the turbulent Schmidt number. An extensive study by Tominaga and Stathopoulos (2007) showed that different values of Sc_t are required for various types of flow fields. Riddle, Carruthers, Sharpe, McHugh, and Stocker (2004) suggested that values of Sc_t lower than 0.7 are appropriate for plume dispersion and we used a value of 0.63 for Sc_t in this study.

With the assumption of an equilibrium boundary layer (Bourdin & Wilson, 2008; Guo & Maghirang, 2012; Richards & Hoxey, 1993; Santiago et al., 2007; Yeh et al., 2010), the inlet values for ε and k may be

calculated as follows:

$$k_{\rm in} = \frac{u_*^2}{\sqrt{C_\mu}} \tag{19}$$

$$\varepsilon_{\rm in} = \frac{u_*^3}{\kappa z},\tag{20}$$

where u_* is the TSV upstream of the vegetation elements (i.e., shrub and grass). The pressure values at the inlet, lower wall, front and back faces were given zero gradients, the upper wall was given a symmetry condition, and a constant value was set for the outlet conditions. As for the other regions in the domain, the outlet flow was given a fully developed flow condition (i.e., zero velocity gradient), symmetry condition at the upperWall, back and front regions, and no-slip condition at the lowerWall, and near-wall conditions for ε and k (i.e., epsilonWallFunction and kqrWallFunction, respectively) for all other domain regions were utilized. The initial values inside the domain (called internalField in OpenFOAM) for all parameters were set to be zero. The wind velocity profiles obtained from field measurements were made as the input values for the x-component inlet velocities (u_x) whereas other velocity components u_{ν} and u_{z} were zero. Simulation was continued until the residual values of 1×10^{-7} that was attained for about 47,000 iterations for the wind speed simulation and about 1,250 iterations for the concentration. The model parameters and their values used in the CFD simulations are provided in Table 1.

3 | RESULTS

3.1 | Particle size distribution (PSD)

The PSDs of soil obtained from underneath the shrub and grass patches are shown in Figure 3. Shrub microsites have soils with the coarsest-grained PSDs, bare interspaces have the finest-grained PSDs, and grass patches have PSDs that are intermediate to the other two types of microsite. The median grain diameters were 341.6, 212.6, and 147.1 μ m for the shrub, grass, and bare microsites, respectively. Statistical tests (One-way ANOVA and Tukey HSD) showed significant differences in median (F=99.34, p<0.01) and mean (F=123.1, p<0.01) grain diameter between the microsites. The increase in

TABLE 1 Model parameters and their values used in the CFD simulations

Parameter	Symbol	Value
Air density (kg m ⁻³)	ρ	1.225
Air dynamic viscosity (kg m ⁻¹ s ⁻¹)	μ	1.79×10^{-5}
Turbulence model constant	$C_{1\varepsilon}$	1.42
Turbulence model constant	$C_{2\varepsilon}$	1.68
Turbulence model constant	C_{μ}	0.085
Turbulence model constant	β	0.012
Turbulence model constant	η_o	4.38
Turbulence Prandtl number for k	σ_k	0.719
Turbulence Prandtl number for $\boldsymbol{\epsilon}$	$\sigma_{arepsilon}$	0.719
Von Karman constant	К	0.4187

Note. CFD = computational fluid dynamics.

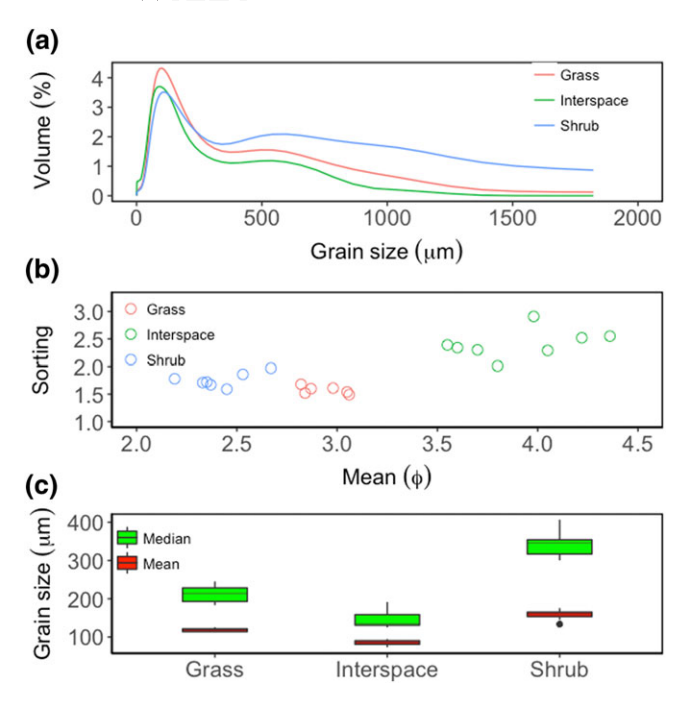


FIGURE 3 (a) Particle size distribution, (b) the mean and median grain size, and (c) sorting and mean of grain size (ϕ) of soils from the microsites (shrub, grass, and bare). The box plot (b) shows the median (solid line); the box enclosure, which represents the interquartile range (first and the third quartiles); and the whiskers, which represent the variability outside the upper and lower quartiles (1.5 times or more the range of variation above the third quartile or more below the first quartile)

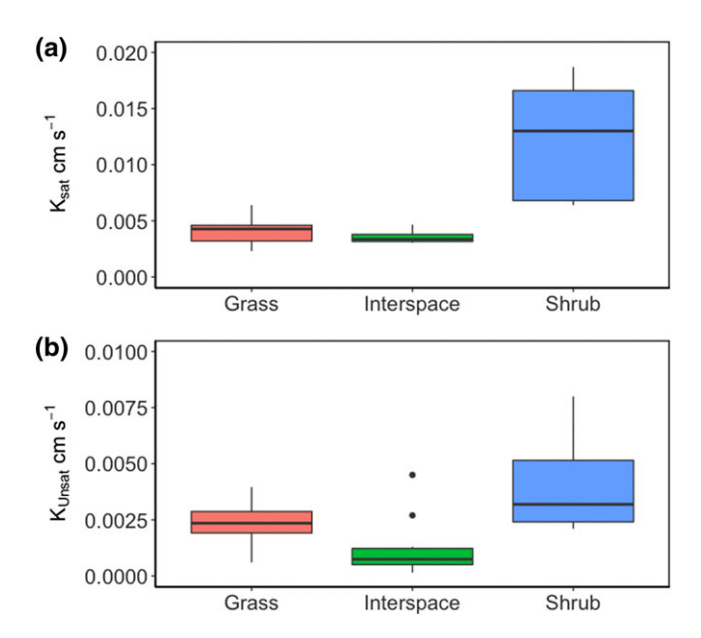
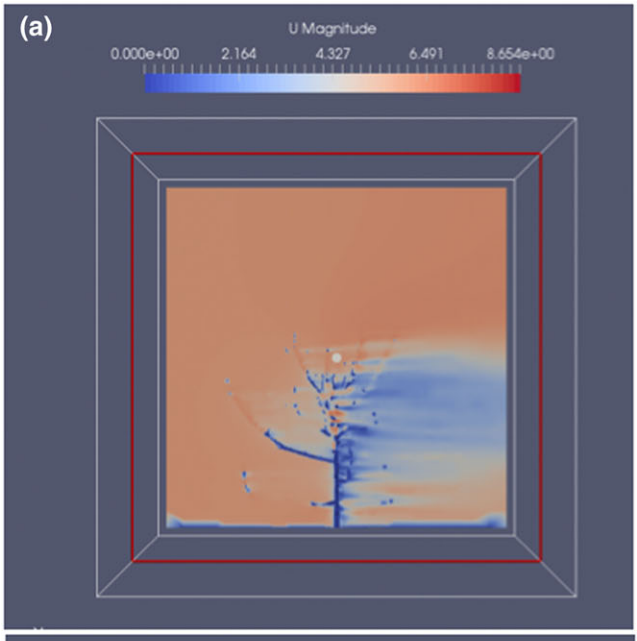


FIGURE 4 Saturated (a) and unsaturated (b) hydraulic conductivity measured under shrub and grass canopies and in bare soil microsites. Each box plot shows the median (solid line); the box enclosure, which represents the interquartile range (first and the third quartiles); and the whiskers, which represent the variability outside the upper and lower quartiles (1.5 times or more the range of variation above the third quartile or more below the first quartile)

sorting with decreased grain diameter mean (ϕ size scale) that is observed among the microsites in Figure 3b is typical for active transport systems.

3.2 | Soil hydrological properties

The results from the infiltrometer experiments show that the saturated (K_{sat}) and unsaturated (K_{unsat}) hydraulic conductivities were consistently higher in the shrub microsites (Figure 4) compared to grass and bare microsites. The dual head infiltrometer measurements showed that the K_{sat} average values were 0.012, 0.004, 0.003 cm s $^{-1}$ for the shrub, grass, and bare microsites, respectively. K_{unsat} values were higher in the shrub microsites as well (Figure 4). The average K_{unsat} values were 0.004, 0.002, and 0.001 cm s $^{-1}$ for shrub, grass,



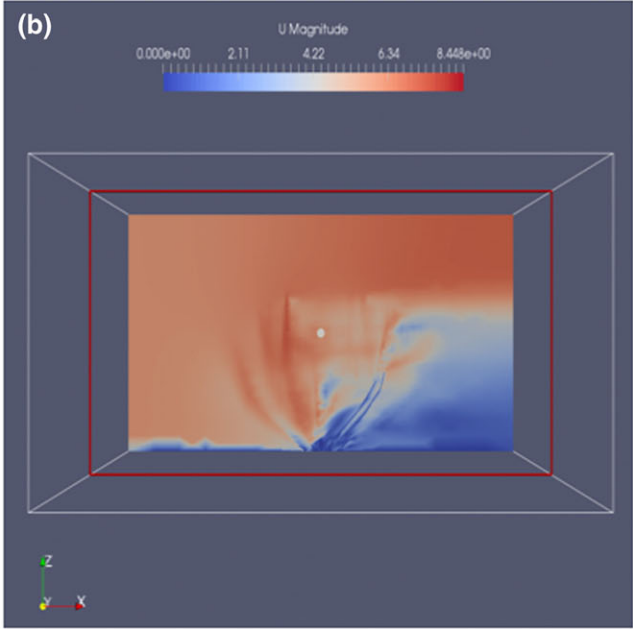


FIGURE 5 Example air flow simulation runs in OpenFOAM®: (a) shrub and (b) grass. Direction of simulated windflow is from left to right. U is the simulated wind velocity in m $\rm s^{-1}$

and bare microsites, respectively. Statistical test showed significant differences in K_{sat} among the microsites (F = 9.16, p = .004). However, Tukey HSD post hoc tests showed that the difference in K_{sat} values specifically between the grass and bare microsites were not significant (p = .97). The K_{unsat} values showed similar trend with significant difference in K_{unsat} between shrub and interspace microsites (p = .001).

3.3 | Numerical simulation

Sliced views (along the centerline) of the 3D contour plots of the wind speed profiles both for the grass and the shrub are shown in Figure 5. The plots show that wind speed reduction occurs along the top of the canopies, and the presence of branches and leaves within the canopies cause a dramatic decrease of wind speed downwind and in the lee of the canopies as shown by the sharp colour change in the contour plots. In Figure 5, maximum wind speed reduction occurs at around

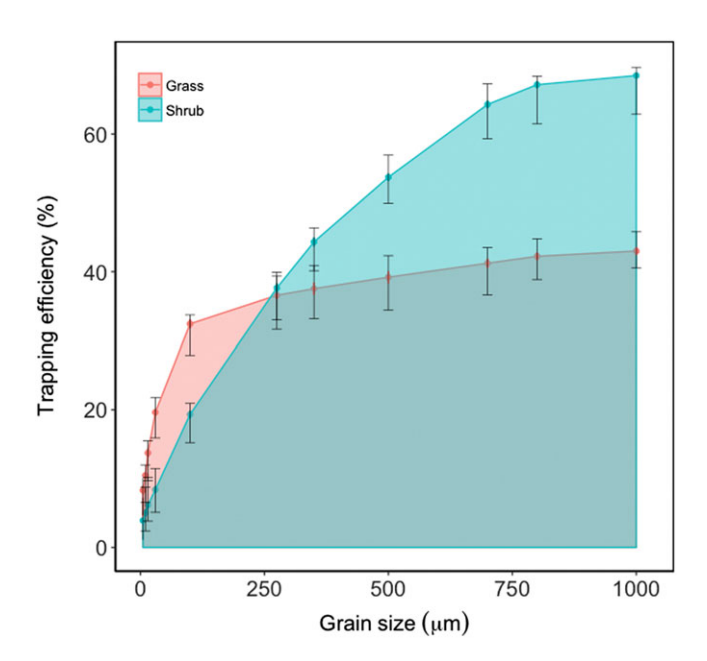


FIGURE 6 Trapping efficiencies of shrub and grass canopies at a constant wind speed of 9 m s⁻¹. The high and low error bars represent the trapping efficiency at 6 and 12 m s⁻¹, respectively

 $0.7H_s$ (height of the shrub) for the shrub while it occurs at $0.2H_g$ (height of the grass) for the grass. The wind profiles are affected by the inherent porosity of the grass and shrub canopies. CFD simulations showed increased trapping efficiencies of both the grass and shrub when subjected to increased wind speeds of 6, 9, and $12~m~s^{-1}$ (Figure 6). This may be attributed to the fact that the motion of vegetation elements was not explicitly incorporated into our numerical simulation. As such, the streamlining phenomenon that occurs for moving vegetation elements that could have lowered the trapping efficiencies especially at higher wind speeds were not encountered (Beckett, Freer-Smith, & Taylor, 2000).

While both shrub and grass tend to be more efficient in trapping coarse sediments, the trapping efficiencies for grasses level off at 33% with a corresponding grain size of approximately 100 um (Figure 6). Additionally, Figure 6 shows that the grass is more efficient for trapping fine-grained particles <250 μ m, but shrubs are more efficient for trapping coarse particles (250–1,000 μ m). Our modelling results also show that the trapping efficiencies for both shrub and grass decreased when the plants are more porous, and the proportion of the sediments trapped by the plants also depend on the grain size of the wind-borne sediments (Figure 7). Collection efficiency varies by particle size to a greater extent for the more-porous shrub than it does for the less-porous grass.

4 | DISCUSSION

This study investigated the applicability of an open-source CFD approach to evaluate the aeolian sediment trapping efficiencies of two species of vegetation associated with the phenomenon of land degradation due to shrub encroachment in a desert grassland. From the CFD simulations and field measurements of PSD and infiltration rates in a grass-shrub ecotone in the Chihuahuan Desert, we infer that trapping of wind eroded sediment by the shrub and grass might contribute to textural changes over time in the underlying soil surface due to the selective size range of particles that each type of vegetation filters out of the air flow. We determined that the less-porous Black Grama grass traps finer particles more efficiently in comparison to the more-porous Creosote shrub, which traps coarser particles

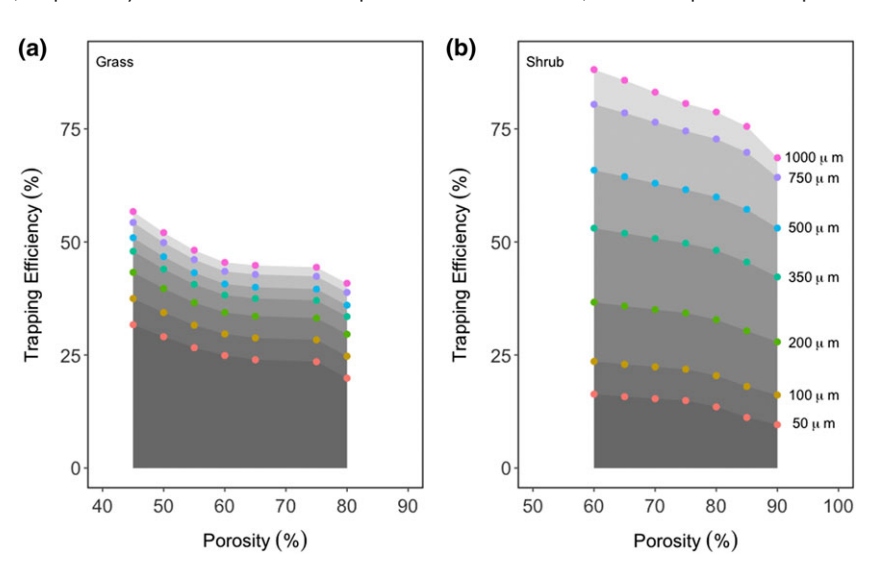


FIGURE 7 Relationships of simulated shrub (a) and grass (b) canopy porosities and trapping efficiencies for different particle sizes of aeolian sediment

more efficiently (Figure 6). Modelling results were supported by our field measurements of soil texture among microsites, which showed that soils underneath shrubs are generally coarser than those of the grasses (Figure 3). Because suspension of particles in desert shrublands predominantly occurs at heights >0.75 m above ground (Breshears et al., 2003), a majority of the aeolian sediment transport within Creosote shrub and Black Grama grass canopies probably occurs via saltation of particles 70-500 µm in diameter (Field et al., 2010; Saxton, Chandler, & Schillinger, 1999). In addition to trapping wind-borne aeolian sediment, the presence of both types of vegetation creates surface roughness and a protective cover to the soil surface that is essential in limiting re-suspension of soil particles and decreasing soil erosion beneath the plant canopies (Zhao, Ma, & Chen, 2007). Although we did not determine the specific mechanism by which the different plant types cause more or less deposition of different sized particles, we speculate that shrub canopies are not only more porous but also have larger pores than grass canopies, thus permitting many fine particles of aeolian sediment to pass through the canopy whereas larger particles are more likely to encounter a leaf, stem, or branch and be removed from the wind stream and deposited on the shrub microsite soil surface.

The primary source of erosion in this environment is via saltation and suspension of finer particles from bare interspace patches in the shrub-grass ecotone (Ravi & D'Odorico, 2009; Sankey, Ravi, et al., 2012). These particles are then deposited beneath and in the lee of grasses and shrubs. The PSD results (Figure 3) showed that the soil surface beneath grasses consisted of a finer distribution of particle sizes whereas the PSD was coarser beneath shrubs. As illustrated with the CFD simulations, this difference in the spatial patterning of soil particles could be related to the more porous nature of the shrub canopies compared to the grass. These modelling results agree with observations of Leenders, Sterk, and Van Boxel (2011), who used an empirical model to predict the amount of trapped particles, as well as Gross (1987), who developed simulations using a homogeneous porosity approach and regularly shaped geometries for the vegetation structures. For our study, we simulated the airflow across the closely resembled geometries of both the Creosote shrub and Black Grama grass. Our simulations, however, did not account for leaf architecture, spatial distribution of leaves, growth stage of the plants, plant-to-plant morphological variations, and seasonal changes of canopy structure (e.g., phenology). Each of these factors may impact the sediment trapping efficiencies of vegetation. Nevertheless, our study presents the first step toward a novel application of the CFD modelling framework.

The wind speed contour plots (Figure 5) showed that the expected behaviour of the normalized wind speed profiles at the wake of the canopy agrees with observations by previous studies (Cionco & Ellefsen, 1998; Endalew et al., 2009; Katul, Mahrt, Poggi, & Sanz, 2004; Pyles, Paw U, & Falk, 2004). The instantaneous increase of wind speeds of the displaced profile at the top and sides of the vegetation canopies was compensated by overflows and wind speeds that increased instantaneously around the plants (Endalew et al., 2009). This region, known as the roughness sublayer (Georgiadis, Dalpane, Rossi, & Nerozzi, 1996), dictates the turbulence in air flow due to the complexity and three-dimensionality of the structure of canopies, and it is also where oscillations in air flow occur. A potential limitation

of this study is that the numerical simulations were completed under the assumption of an equilibrium boundary layer in order to simplify equations and numerical simulations. Moreover, our numerical simulation did not incorporate a reduction in trapping efficiency due to vegetation motion (Beckett et al., 2000); however, our results showed increased particle trapping by vegetation with increased wind speed which could be explained by the obstruction of air flow due to (rigid) vegetation and gravitational settling of sediment due to reduced capacity of air to carry dust leeward of the plant (Hoffmann, Funk, Wieland, Li, & Sommer, 2008). A potentially confounding issue is that the increased windspeed might actually result in less deposition directly beneath the plant since the most rapid flow might be expected to transport the grains farther in a horizontal direction as they fall slowly downward (i.e., in the lee of, as opposed to directly beneath, the plant). It is interesting to compare where the simulated maximum reduction of velocity occurs within the obstructed flow on the downwind side of the grass and shrub. For the shrub, a majority of the vegetative elements responsible for wind speed reduction are located in the upper canopy portion of the plant compared to the lower portion that is mostly composed of the trunk and stems. The grass, on the other hand, forms a tighter bunch of stalks and blades that reduce wind speed especially near to base of the plant (Figure 5).

Our results also highlight the significance of sediment trapping in structuring patch-scale soil properties and ecohydrological processes. Despite the fact that we only considered the rigid structure of both canopies, the CFD model demonstrated differential trapping efficiencies between the grass and shrub. This is primarily due to the difference in the structure and porosity of the shrub and grass that dictated the soil particle transport across both vegetation types, as well as the size ranges of soil particles present beneath each vegetation type.

Land degradation induced by shrub encroachment is characterized by a decline in structural connectivity which can exert a dominant control on shrub establishment in grasslands (D'Odorico, Bhattachan, Davis, Ravi, & Runyan, 2013; Okin et al., 2009; Turnbull et al., 2012). Increases in the length of connected pathways (functional connectivity) in these landscapes trigger a self-sustained cycle of soil erosion and resource depletion, whereas the vegetation canopies can capture sediments transported by wind and water resulting in the formation of fertile shrub patches (Schlesinger et al., 1990). In landscapes at the early stages of the encroachment processes, with coexistence of shrub, grass and bare soil microsites, the differential trapping of sediments by shrub and grass canopies may be an important factor controlling the variability of hydrologic processes in the vegetated microsites. The shrub canopies, by trapping coarser particles in comparison to grass canopies, can maintain higher infiltration rates in the shrub microsites. Higher infiltration rates in turn might result in faster development of shrub fertile islands with enhanced ecological productivity, whereas in the case of grass islands the accumulation of fine particles might result in lower water infiltration. In desert grasslands that are subject to increased wind erosion as a result of shrub encroachment (Ravi & D'Odorico, 2009; Sankey, Ravi, et al., 2012), the vegetation change over time might result in (a) a reduction in grass canopies that efficiently capture the finest-grained aeolian particles, (b) an increase in bare interspaces where wind erosion occurs, and

(c) an increase in porous shrub canopies that are most efficient at trapping coarse aeolian sediments. These changes in aeolian-vegetation dynamics due to shrub encroachment over time produce a landscape with more shrub soil microsites with greater water infiltration capacity. Notably, there are also many desert shrublands that are subjected to increased wind erosion as a result of type conversion from shrubland to grassland due to disturbance of fire and invasive grasses (Miller, Bowker, Reynolds, & Goldstein, 2012; Sankey, Germino, & Glenn, 2009; Sankey, Germino, et al., 2012). Thus, the CFD approach we demonstrated here is likely well-suited for quantifying trapping efficiencies and elucidating ecohydrological implications of vegetation-aeolian dynamics associated with land degradation worldwide in ecosystems undergoing transitions from grassland to shrubland or vice versa.

5 | CONCLUSION

Results of field observations and CFD modelling provided complementary evidence that shrubs are more efficient in trapping coarse grained wind-borne sediments whereas grasses selectively capture more fine particles in a grass-shrub transition zone in the Chihuahuan Desert. The differential trapping of aeolian sediments by vegetation canopies could have important ecological and hydrological implications in that it might result in textural changes beneath the vegetation and thus, for example, affect the competition between shrubs and grasses. Our study represents the first attempt to evaluate the effect of porosities corresponding to 3D canopy structure models of both shrub and grass in a heterogeneous arid landscape and to validate their size-selective trapping efficiencies of wind-borne sediments.

ACKNOWLEDGEMENTS

This research was funded by the U.S. National Science Foundation (NSF) Award EAR-1451518 for S. Ravi, Award EAR-1451489 for J. Li. The authors gratefully acknowledge the contributions of Jon Erz & Andy Lopez (FWS, SNWR), Scott Collins, and Amaris Swan (Sevilleta LTER, New Mexico, USA) for providing access to field and laboratory facilities and technical guidance. This manuscript is submitted for publication with the understanding that the U.S. Government is authorized to reproduce and distribute reprints for Governmental purposes. Any use of trade, product, or firm names is for descriptive purposes only and does not imply endorsement by the U.S. Government.

ORCID

Sujith Ravi http://orcid.org/0000-0002-0425-9373

Junran Li http://orcid.org/0000-0001-7837-641X

Joel B. Sankey http://orcid.org/0000-0003-3150-4992

REFERENCES

- Archer, S., Schimel, D. S., & Holland, E. A. (1995). Mechanisms of shrubland expansion: Land use, climate or CO2? *Climatic Change*, 29(1), 91–99. https://doi.org/10.1007/BF01091640
- Beckett, K. P., Freer-Smith, P. H., & Taylor, G. (2000). Particulate pollution capture by urban trees: Effect of species and windspeed. *Global Change Biology*, 6(8), 995–1003. https://doi.org/10.1046/j.1365-2486.2000.00376.x

- Bhark, E. W., & Small, E. E. (2003). Association between plant canopies and the spatial patterns of infiltration in shrubland and grassland of the Chihuahuan Desert, New Mexico. *Ecosystems*, 6(2), 185–196. https:// doi.org/10.1007/s10021-002-0210-9
- Bitog, J. P., Lee, I.-B., Hwang, H.-S., Shin, M.-H., Hong, S.-W., Seo, I.-H., ... Pang, Z. (2012). Numerical simulation study of a tree windbreak. Biosystems Engineering, 111(1), 40–48. https://doi.org/10.1016/j. biosystemseng.2011.10.006
- Bourdin, P., & Wilson, J. D. (2008). Windbreak Aerodynamics: Is computational fluid dynamics reliable? *Boundary-Layer Meteorology*, 126(2), 181–208. https://doi.org/10.1007/s10546-007-9229-y
- Breshears, D. D., Whicker, J. J., Johansen, M. P., & Pinder, J. E. (2003). Wind and water erosion and transport in semi-arid shrubland, grassland and forest ecosystems: Quantifying dominance of horizontal wind-driven transport. Earth Surface Processes and Landforms, 28(11), 1189–1209. https://doi.org/10.1002/esp.1034
- Charley, J. L., & West, N. E. (1977). Micro-patterns of nitrogen mineralization activity in soils of some shrub-dominated semi-desert ecosystems of Utah. Soil Biology and Biochemistry, 9(5), 357–365. https://doi.org/10.1016/0038-0717(77)90010-4
- Cheng, Y., Lien, F. S., Yee, E., & Sinclair, R. (2003). A comparison of large Eddy simulations with a standard k–ε Reynolds-averaged Navier–Stokes model for the prediction of a fully developed turbulent flow over a matrix of cubes. *Journal of Wind Engineering and Industrial Aerodynamics*, *91*(11), 1301–1328. https://doi.org/10.1016/j.jweia.2003.08.001
- Cionco, R. M., & Ellefsen, R. (1998). High resolution urban morphology data for urban wind flow modeling. *Atmospheric Environment*, 32(1), 7–17. https://doi.org/10.1016/S1352-2310(97)00274-4
- Coetzee, B. W. T., Tincani, L., Wodu, Z., & Mwasi, S. M. (2008). Overgrazing and bush encroachment by Tarchonanthus camphoratus in a semi-arid savanna. *African Journal of Ecology*, 46(3), 449–451. https://doi.org/10.1111/j.1365-2028.2007.00842.x
- D'Odorico, P., Bhattachan, A., Davis, K. F., Ravi, S., & Runyan, C. W. (2013). Global desertification: Drivers and feedbacks. Advances in Water Resources, 51, 326–344. https://doi.org/10.1016/j.advwatres.2012.01.013
- Dukes, D., Gonzales, H. B., Ravi, S., Grandstaff, D. E., Van Pelt, R. S., Li, J., ... Sankey, J. B. (2018). Quantifying postfire aeolian sediment transport using rare earth element tracers. *Journal of Geophysical Research: Biogeosciences*, 123. https://doi.org/10.1002/2017JG004284
- Endalew, A. M., Hertog, M., Delele, M. A., Baetens, K., Persoons, T., Baelmans, M., ... Verboven, P. (2009). CFD modelling and wind tunnel validation of airflow through plant canopies using 3D canopy architecture. *International Journal of Heat and Fluid Flow*, 30(2), 356–368. https://doi.org/10.1016/j.ijheatfluidflow.2008.12.007
- Field, J. P., Belnap, J., Breshears, D. D., Neff, J. C., Okin, G. S., Whicker, J. J., ... Reynolds, R. L. (2010). The ecology of dust. Frontiers in Ecology and the Environment, 8(8), 423–430. https://doi.org/10.1890/090050
- Folk, R. L. (1980). Petrology of sedimentary rocks. Austin, TX: Hemphill Publishing Company.
- Georgiadis, T., Dalpane, E., Rossi, F., & Nerozzi, F. (1996). Orchard-atmosphere physical exchanges: Modelling the canopy aerodynamics. In *Acta Horticulturae* (pp. 177–182). Leuven, Belgium: International Society for Horticultural Science (ISHS). doi:https://doi.org/10.17660/ActaHortic.1996.416.21
- Gromke, C., Buccolieri, R., Di Sabatino, S., & Ruck, B. (2008). Dispersion study in a street canyon with tree planting by means of wind tunnel and numerical investigations—Evaluation of CFD data with experimental data. *Atmospheric Environment*, 42(37), 8640–8650. https://doi.org/10.1016/j.atmosenv.2008.08.019
- Gross, G. (1987). A numerical study of the air flow within and around a single tree. *Boundary-Layer Meteorology*, 40(4), 311–327. https://doi.org/10.1007/BF00116099
- Guo, L., & Maghirang, R. G. (2012). Numerical simulation of airflow and particle collection by vegetative barriers. *Engineering Applications*

- of Computational Fluid Mechanics, 6(1), 110–122. https://doi.org/10.1080/19942060.2012.11015407
- He, Y., D'Odorico, P., De Wekker, S. F. J., Fuentes, J. D., & Litvak, M. (2010). On the impact of shrub encroachment on microclimate conditions in the northern Chihuahuan desert. *Journal of Geophysical Research-Atmospheres*, 115(D21). https://doi.org/10.1029/2009JD013529
- Hoffmann, C., Funk, R., Wieland, R., Li, Y., & Sommer, M. (2008). Effects of grazing and topography on dust flux and deposition in the Xilingele grassland, Inner Mongolia. *Journal of Arid Environments*, 72(5), 792–807. https://doi.org/10.1016/j.jaridenv.2007.09.004
- Hoover, A. N., & Germino, M. J. (2012). A common-garden study of resource-island effects on a native and an exotic, annual grass after fire. Rangeland Ecology & Management, 65, 160–170. https://doi.org/ 10.2111/RFM-D-11-00026.1
- Huxman, T. E., Wilcox, B. P., Breshears, D. D., Scott, R. L., Snyder, K. A., Small, E. E., ... Jackson, R. B. (2005). Ecohydrological implications of woody plant encroachment. *Ecology*, 86(2), 308–319. https://doi.org/10.1890/03-0583
- Katul, G. G., Mahrt, L., Poggi, D., & Sanz, C. (2004). ONE- and TWO-equation models for canopy turbulence. Boundary-Layer Meteorology, 113(1), 81–109. https://doi.org/10.1023/B: BOUN.0000037333.48760.e5
- Lee, I. B., Sase, S., & Sung, S. H. (2007). Evaluation of CFD accuracy for the ventilation study of a naturally ventilated broiler house. *Japan Agricultural Research Quarterly: JARQ*, 41(1), 53–64. https://doi.org/ 10.6090/jarq.41.53
- Lee, S.-J., & Lim, H.-C. (2001). A numerical study on flow around a triangular prism located behind a porous fence. *Fluid Dynamics Research*, 28(3), 209–221. https://doi.org/10.1016/S0169-5983(00)00030-7
- Leenders, J. K., Sterk, G., & Van Boxel, J. H. (2011). Modelling wind-blown sediment transport around single vegetation elements. *Earth Surface Processes and Landforms*, 36(9), 1218–1229. https://doi.org/10.1002/esp.2147
- Li, J., Okin, G. S., Alvarez, L., & Epstein, H. (2007). Quantitative effects of vegetation cover on wind erosion and soil nutrient loss in a desert grassland of southern New Mexico, USA. *Biogeochemistry*, 85(3), 317–332.
- Li, J., Okin, G. S., Alvarez, L., & Epstein, H. (2009). Sediment deposition and soil nutrient heterogeneity in two desert grassland ecosystems, southern New Mexico. *Plant and Soil*, 319, 67–84. https://doi.org/10.1007/s11104-008-9850-7
- Li, J., Okin, G. S., Alvarez, L., & Epstein, H. (2008). Effects of wind erosion on the spatial heterogeneity of soil nutrients in two desert grassland communities. *Biogeochemistry*, 88, 73–88. https://doi.org/10.1007/ s10533-008-9195-6
- Li, J., Okin, G. S., Herrick, J. E., Belnap, J., Munson, S. M., & Miller, M. E. (2010). A simple method to estimate threshold friction velocity of wind erosion in the field. *Geophysical Research Letters*, 37(10). n/a-n/a. doi: https://doi.org/10.1029/2010GL043245
- Li, J., & Ravi, S. (2018). Interactions among hydrological-aeolian processes and vegetation determine grain-size distribution of sediments in a semi-arid coppice dune (nebkha) system. *Journal of Arid Environments*, 154, 24–33. https://doi.org/10.1016/j.jaridenv.2018.03.011
- Li, W., Wang, F., & Bell, S. (2007). Simulating the sheltering effects of windbreaks in urban outdoor open space. *Journal of Wind Engineering and Industrial Aerodynamics*, 95(7), 533–549. https://doi.org/10.1016/j.jweia.2006.11.001
- Lin, X. J., Barrington, S., Choinière, D., & Prasher, S. (2007). Simulation of the effect of windbreaks on odour dispersion. *Biosystems Engineering*, 98(3), 347–363. https://doi.org/10.1016/j. biosystemseng.2007.07.010
- Miller, M. E., Bowker, M. A., Reynolds, R. L., & Goldstein, H. L. (2012). Post-fire land treatments and wind erosion—Lessons from the Milford Flat Fire, UT, USA. Aeolian Research, 7(C), 29–44. https://doi.org/ 10.1016/j.aeolia.2012.04.001

- Muldavin, E. H. (2002). Some floristic characteristics of the northern Chihuahuan Desert: A search for its northern boundary. *Taxon*. Retrieved from http://www.ingentaconnect.com/content/iapt/tax/2002/00000051/00000003/art00003
- Nimmo, J. R., Schmidt, K. M., Perkins, K. S., & Stock, J. D. (2009). Rapid measurement of field-saturated hydraulic conductivity for areal characterization. *Vadose Zone Journal*, 8, 142–149. https://doi.org/10.2136/ vzj2007.0159
- Okin, G. S., & Gillette, D. A. (2001). Distribution of vegetation in wind-dominated landscapes: Implications for wind erosion modeling and landscape processes. *Journal of Geophysical Research-Atmospheres*, 106(D9), 9673–9683. https://doi.org/10.1029/2001JD900052
- Okin, G. S., Parsons, A. J., Wainwright, J., Herrick, J. E., Bestelmeyer, B. T., Peters, D. C., & Fredrickson, E. L. (2009). Do changes in connectivity explain desertification? *BioScience*, *59*(3), 237–244. https://doi.org/10.1525/bio.2009.59.3.8
- OpenFOAM (2015). https://openfoam.org/
- Packwood, A. R. (2000). Flow through porous fences in thick boundary layers: Comparisons between laboratory and numerical experiments. *Journal of Wind Engineering and Industrial Aerodynamics*, 88(1), 75–90. https://doi.org/10.1016/S0167-6105(00)00025-8
- Puigdefabregas, J. (2005). The role of vegetation patterns in structuring runoff and sediment fluxes in drylands. *Earth Surface Processes and Landforms*, 30(2), 133–147. https://doi.org/10.1002/esp.1181
- Pyles, R. D., Paw U, K. T., & Falk, M. (2004). Directional wind shear within an old-growth temperate rainforest: Observations and model results. *Agricultural and Forest Meteorology*, 125(1–2), 19–31. https://doi.org/10.1016/j.agrformet.2004.03.007
- Raupach, M. R., Woods, N., Dorr, G., Leys, J. F., & Cleugh, H. A. (2001). The entrapment of particles by windbreaks. *Atmospheric Environment*, 35(20), 3373. Retrieved from http://www.sciencedirect.com/science/ article/B6VH3-439VC0B-P/2/ 25a8c69832935b48ae9c1f0a790f0fd0-3383.
- Ravi, S., Breshears, D. D., Huxman, T. E., & D'Odorico, P. (2010). Land degradation in drylands: Interactions among hydrologic-aeolian erosion and vegetation dynamics. *Geomorphology*, 116(3–4), 236–245. https://doi.org/10.1016/j.geomorph.2009.11.023
- Ravi, S., & D'Odorico, P. (2009). Post-fire resource redistribution and fertility island dynamics in shrub encroached desert grasslands: A modeling approach. *Landscape Ecology*, 24(3), 325–335. https://doi. org/10.1007/s10980-008-9307-7
- Ravi, S., D'Odorico, P., Breshears, D. D., Field, J. P., Goudie, A. S., Huxman, T. E., ... Zobeck, T. M. (2011). Aeolian processes and the biosphere. Reviews of Geophysics, 49(3). https://doi.org/10.1029/2010RG000328
- Ravi, S., D'Odorico, P., & Okin, G. S. (2007). Hydrologic and aeolian controls on vegetation patterns in arid landscapes. *Geophysical Research Letters*, 34(24). https://doi.org/10.1029/2007GL031023
- Reynolds, W. D., & Elrick, D. E. (1990). Ponded infiltration from a single ring: I. Analysis of steady flow. Soil Science Society of America Journal, 54(5), 1233. https://doi.org/10.2136/sssaj1990.0361599500540005 0006x
- Richards, P. J., & Hoxey, R. P. (1993). Appropriate boundary conditions for computational wind engineering models using the k-ε turbulence model. *Journal of Wind Engineering and Industrial Aerodynamics*, 46-47(Supplement C), 145-153. https://doi.org/10.1016/0167-6105(93)90124-7
- Riddle, A., Carruthers, D., Sharpe, A., McHugh, C., & Stocker, J. (2004). Comparisons between FLUENT and ADMS for atmospheric dispersion modelling. Atmospheric Environment, 38(7), 1029–1038. https://doi. org/10.1016/j.atmosenv.2003.10.052
- Rosenfeld, M., Marom, G., & Bitan, A. (2010). Numerical simulation of the airflow across trees in a windbreak. *Boundary-Layer Meteorology*, 135(1), 89–107. https://doi.org/10.1007/s10546-009-9461-8
- Sankey, J. B., Germino, M. J., & Glenn, N. F. (2009). Aeolian sediment transport following wildfire in sagebrush steppe. *Journal of Arid Environ*ments, 73(10), 912–919.

- Sankey, J. B., Germino, M. J., Sankey, T. T., & Hoover, A. N. (2012). Fire effects on the spatial patterning of soil properties in sagebrush steppe, USA: A meta-analysis. *International Journal of Wildland Fire*, 21(5), 545–556. https://doi.org/10.1071/WF11092
- Sankey, J. B., Law, D. J., Breshears, D. D., Munson, S. M., & Webb, R. H. (2013). Employing lidar to detail vegetation canopy architecture for prediction of aeolian transport. *Geophysical Research Letters*, 40(9), 1724–1728. https://doi.org/10.1002/grl.50356
- Sankey, J. B., Ravi, S., Wallace, C. S. A., Webb, R. H., & Huxman, T. E. (2012). Quantifying soil surface change in degraded drylands: Shrub encroachment and effects of fire and vegetation removal in a desert grassland. *Journal of Geophysical Research Biogeosciences*, 117(2). https://doi.org/10.1029/2012JG002002
- Santiago, J. L., Martín, F., Cuerva, A., Bezdenejnykh, N., & Sanz-Andrés, A. (2007). Experimental and numerical study of wind flow behind windbreaks. Atmospheric Environment, 41(30), 6406–6420. https://doi.org/10.1016/j.atmosenv.2007.01.014
- Saxton, K., Chandler, D., & Schillinger, W. (1999). Wind erosion and air quality research in the northwest U.S. Columbia plateau: Organization and progress. In E.E. Stott, R.H. Mohtar, and G.C. Steinhardt (eds). Sustaining the Global Farm - Selected papers from the 10th International Soil Conservation Organization Meeting, 24-29 May, West Lafayette, IN.
- Schlesinger, W. H., Reynolds, J. F., Cunningham, G. L., Huenneke, L. F., Jarrell, W. M., Virginia, R. A., & Whitford, W. G. (1990). Biological feedbacks in global desertification. *Science (New York, N.Y.)*, 247(4946), 1043–1048. https://doi.org/10.1126/science.247.4946.1043
- Scholes, R. J., & Archer, S. R. (1997). Tree-grass interactions in savannas. Annual Review of Ecology and Systematics, 28(1), 517–544. https://doi.org/10.1146/annurev.ecolsys.28.1.517
- Tiwary, A., Morvan, H. P., & Colls, J. J. (2006). Modelling the size-dependent collection efficiency of hedgerows for ambient aerosols. Journal of Aerosol Science, 37(8), 990–1015. https://doi.org/10.1016/j.jaerosci.2005.07.004
- Tominaga, Y., & Stathopoulos, T. (2007). Turbulent Schmidt numbers for CFD analysis with various types of flowfield. *Atmospheric Environment*, 41(37), 8091–8099. https://doi.org/10.1016/j.atmosenv.2007.06.054

- Turnbull, L., Wilcox, B. P., Belnap, J., Ravi, S., D'Odorico, P., Childers, D., ... Sankey, T. (2012). Understanding the role of ecohydrological feedbacks in ecosystem state change in drylands. *Ecohydrology*, *5*(2), 174–183. https://doi.org/10.1002/eco.265
- Van Auken, O. W. (2000). Shrub invasions of North American semiarid grasslands. Annual Review of Ecology and Systematics, 31(1), 197–215. https://doi.org/10.1146/annurev.ecolsys.31.1.197
- Wang, G., Li, J., Ravi, S., Dukes, D., Gonzales, H. B., & Sankey, J. B. (2018). Post-fire redistribution of soil carbon and nitrogen at a grassland-shrubland ecotone. *Ecosystems*. https://doi.org/10.1007/s10021-018-0260-2
- Wilcox, B. P., & Thurow, T. L. (2006). Emerging issues in rangeland ecohydrology: Vegetation change and the water cycle. Rangeland Ecology & Management, 59(2), 220–224. https://doi.org/10.2111/05-090R1 1
- Wolfe, S. A., & Nickling, W. G. (1993). The protective role of sparse vegetation in wind erosion. *Progress in Physical Geography*, 17(1), 50–68. https://doi.org/10.1177/030913339301700104
- Yeh, C. P., Tsai, C.-H., & Yang, R. J. (2010). An investigation into the sheltering performance of porous windbreaks under various wind directions. *Journal of Wind Engineering and Industrial Aerodynamics*, 98(10), 520–532. https://doi.org/10.1016/j.jweia.2010.04.002
- Zhang, R. D. (1997). Determination of soil sorptivity and hydraulic conductivity from the disk infiltrometer. Soil Science Society of America Journal, 61(4), 1024–1030.
- Zhao, Y. L., Ma, S. S., & Chen, Z. (2007). Aerodynamic roughness of vegetation coverage surface and its influence on soil erosion by the wind tunnel. *Journal of Agricultural Mechanization Research*, 2, 36–39.

How to cite this article: Gonzales HB, Ravi S, Li J, Sankey JB. Ecohydrological implications of aeolian sediment trapping by sparse vegetation in drylands. *Ecohydrology*. 2018;11:e1986. https://doi.org/10.1002/eco.1986